Experimental and numerical investigation of hydro power generator ventilation

H Jamshidi[1], H Nilsson[2] and V Chernoray[3]

[1,2,3]Chalmers University of Technology, SE-412 96 Gothenburg, Sweden

E-mail: hamed.jamshidi@chalmers.se

Abstract. Improvements in ventilation and cooling offer means to run hydro power generators at higher power output and at varying operating conditions. The electromagnetic, frictional and windage losses generate heat. The heat is removed by an air flow that is driven by fans and/or the rotor itself. The air flow goes through ventilation channels in the stator, to limit the electrical insulation temperatures. The temperature should be kept limited and uniform in both time and space, avoiding thermal stresses and hot-spots. For that purpose it is important that the flow of cooling air is distributed uniformly, and that flow separation and recirculation are minimized. Improvements of the air flow properties also lead to an improvement of the overall efficiency of the machine. A significant part of the windage losses occurs at the entrance of the stator ventilation channels, where the air flow turns abruptly from tangential to radial. The present work focuses exclusively on the air flow inside a generator model, and in particular on the flow inside the stator channels. The generator model design of the present work is based on a real generator that was previously studied. The model is manufactured taking into consideration the needs of both the experimental and numerical methodologies. Computational Fluid Dynamics (CFD) results have been used in the process of designing the experimental set-up. The rotor and stator are manufactured using rapid-prototyping and plexi-glass, yielding a high geometrical accuracy, and optical experimental access. A special inlet section is designed for accurate air flow rate and inlet velocity profile measurements. The experimental measurements include Particle Image Velocimetry (PIV) and total pressure measurements inside the generator. The CFD simulations are performed based on the OpenFOAM CFD toolbox, and the steady-state frozen rotor approach. Specific studies are performed, on the effect of adding "pick-up" to spacers, and the effects of the inlet fan blades on the flow rate through the model. The CFD results capture the experimental flow details to a reasonable level of accuracy.

1. Introduction

Hydro power generators are low speed machines with large diameters. They play an important role in the electric power system due to their many advantages, such as their simple design, quick response to load variation, low cost for long service life, and high reliability. The main components of a typical generator are the stator, the rotor, and the conductor coils. Air-Cooling, also known as ventilation-cooling, is the standard and most common cooling concept for small to large electric generators. The stator is made from segments of laminated packets. Spacers are arranged between some segment layers, to form duct passages for the flow of cooling air. An air gap of 20-25 mm is provided between the rotor and the stator. Fans are usually mounted on the rotor to supply air for cooling purposes [1]. In

high-capacity machines there could be axial or centrifugal fans depending on the requirements. Coolers are mounted at the outer periphery of the generator, to cool the hot air with a secondary medium.

The process of conversion of the mechanical energy into electricity in hydro power generators includes four main classes of energy losses [2], electric losses, magnetic losses and mechanical losses. Mechanical losses are mainly due to the flow of cooling air (windage loss), and friction in bearings. The windage losses account for about 20-40% of the total losses of large hydro power generators. All these losses also generate heat, which consequently raises the temperature of the machine components and leads to a change in the material properties. High or varying temperatures may result in a lower efficiency and affect the lifetime of certain components and thus the maintenance requirements of the generator. It is therefore important to remove the heat to keep the generator at a stable, uniform and limited temperature, while keeping the windage losses to a minimum [3]. Improvements in ventilation and cooling methods offer means to run the machines at higher rating without any major modifications in the civil structures and without major investments.

Thermal simulations of electric generators can be divided into thermal networks and Computational Fluid Dynamics (CFD). The thermal network approach has the advantage of being very fast. The accuracy of this method is however strongly dependent on the underlying empirical thermal parameters, in particular the convective heat transfer correlations. In most cases, experimental data must be used to calibrate the thermal network models in order to get sufficiently accurate results. Due to the complex geometries and flow field, this method is only a crude estimate of the situation in the electrical machine. CFD, on the other hand, offers a good potential to fully predict ventilation and cooling in generators [4, 8-11]. CFD has the advantage that it can be used to predict the flow and heat transfer in complex regions. Accurate CFD results can be used for improving the thermal network algorithms without the need for costly experiments. This can provide the possibility to optimize the thermal design of machines at an early stage without the need for extensive and costly experimentation. However, the designers need to have confidence in the use of CFD, so research must be done to validate the CFD modeling results. Further, CFD requires specific skills and access to sufficient computational resources.

There are very few available studies performed on the flow of cooling air in electric generators. Toussaint et al. [5] presented different simulation strategies to numerically compute the flow field in electric generators. Moradnia et al. [8-11], performed steady-state frozen rotor simulations of a simplified electric generator and validate the results with experimental measurements. Gunabushanam et al. [7] investigated the cooling air flow losses in an electric generator model experimentally and numerically. Pickering et al. [6] experimentally and numerically investigated the air flow and heat transfer in a salient pole machine.

The current study aims at a better phenomenological understanding of the flow of cooling air, and its associated losses, in electric generators. A proper representation of the flow of the cooling air is essential before the convective heat transfer should be included in the simulations. The work is based on both experimental and CFD studies of an electric generator model that is specifically designed for the purpose of ventilation studies. New geometrical modifications are introduced, to get a higher mass flow and better flow properties.

2. Geometry Specifications and Operational Conditions

The geometry used in the present work is a half-scale model of the electric generator studied by Moradnia et al. [8-11]. Figure 1 shows the experimental rig and the CAD model of the generator used in the present work. The generator model has 12 poles, a fan attached on top of the rotor, 4 rows of stator cooling channels along the axis of rotation, and 108 cooling channels and coils in each row. The stator height is 0.175m. The rotor tip radius and the stator inner and outer radii are 0.178, 0.1825 and 0.219m, respectively. The height of the stator channels is 4.7mm. The rotational speed of the rotor is 2000rpm to preserve the Reynolds number of the original electric generator. The air flow is driven exclusively by the rotor rotation, with its co-rotating fan.
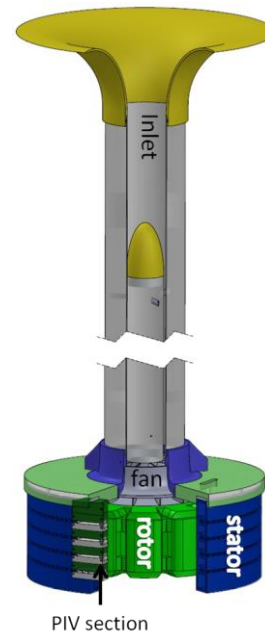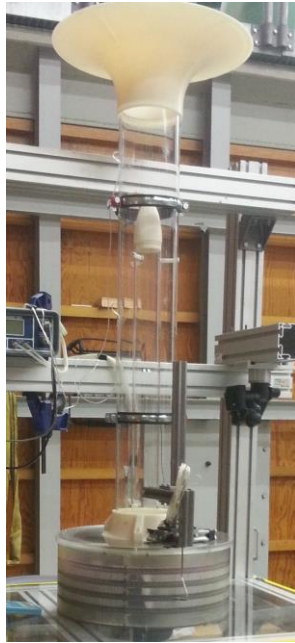
Figure 1 Left: Experimental rig with manometer and total pressure measurement rake. Right: CAD model

The experimental rig is exclusively designed and manufactured for detailed measurements of the flow of cooling air, and is adapted for Particle Image Velocimetry (PIV) and pressure measurements. The geometry of the rotor and stator are slightly simplified with the purpose of improving the accuracy of experimental results, and for preparing for the high-quality CFD simulations. The rotor and stator are manufactured using a rapid prototyping method. The rotor, see figure 2(a), is manufactured using a Stereo Laser Sintering (SLS) process, since it has to withstand large centrifugal forces. To suppress the intensive radiation scattered from the laser sheet by dust particles on the surfaces, the rotor is coated by reflective and absorbing paint (not shown here). The stator, see figure 2(b), is manufactured using a Stereo Lithography Apparatus (SLA) process as it has better surface finish, lower tolerance and higher accuracy. A small section of the stator is manufactured from separately milled Plexiglas parts in order to have a transparent column for PIV measurements.

(a)

(b)

Figure 2 (a) Rotor. (b) Stator with PIV section

Figure 3 shows a cross-section of the generator model, and the layout of the stator channels. The generator used in this work is axially cooled, i.e. the flow of cooling air is axial in the rotor-stator air gap. Figure 3(a) shows that the air enters the machine through the fan at the top, and leaves the machine radially, through the stator channels. The bottom is closed.

The same geometry is used in the numerical simulation, see figure 4. The number of stator cooling channels and coils in each row (108) is divisible by the number of rotor poles and fan blades (12). The computational domain can thus be reduced to a 1/12 sector in the tangential direction, including 9

cooling channels in each channel row and one rotor pole, while employing cyclic boundary conditions at the sides of the domain.
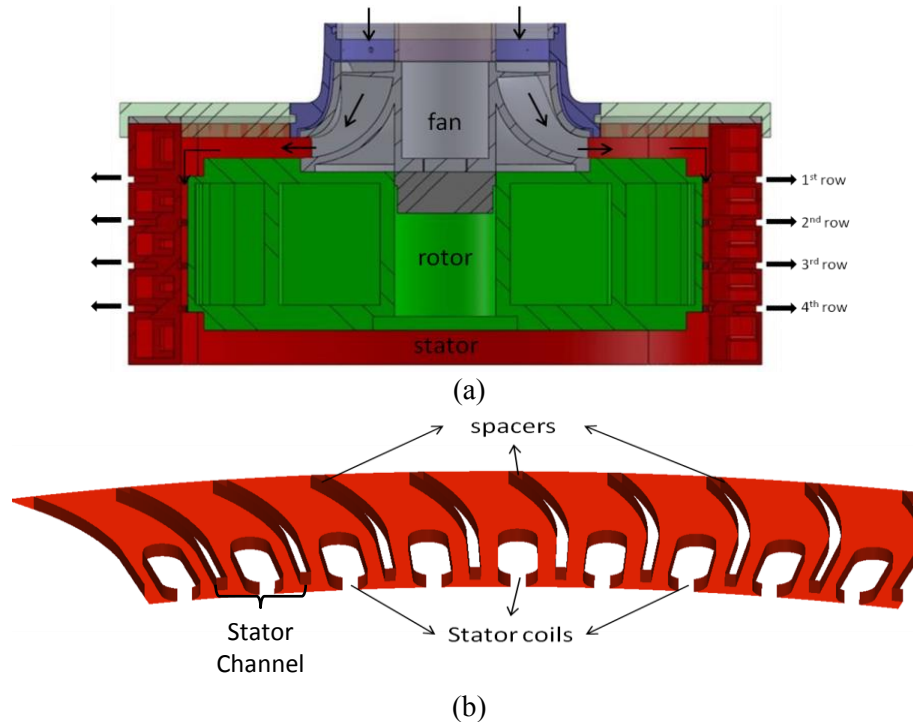

(a)

(b)

Figure 3 (a) Cross-section of the generator model. (b) Stator channels, coils and spacers

2.1. Inlet Section Design

The inlet section, see figure 1, is designed to give a controlled inlet velocity distribution, and to facilitate accurate flow rate measurements. These parts are manufactured using PolyJet 3D printing which leads to smooth surfaces and high axisymmetric precision. They are attached to Plexiglas pipes. The inlet section includes a contraction part, before and after which the static pressure is measured. The acquired pressure difference is used to determine the mean velocity and the volume flow rate. Figure 5(a) shows the relation between the volume flow rate and the square root of the pressure difference. To derive this relation, several CFD simulations were done with different inlet flow rate conditions. A curve fitting resulted in figure 5(a). Figure 5(b) shows a comparison of the CFD results with 5-hole probe measurements, just before the fan. There is a good agreement between the numerical and experimental results. The measurements were taken at 2000rpm rotor rotational speed, yielding a flow rate of 0.157m^3/s. The numerical simulations are done using OpenFOAM and the steady-state SIMPLE algorithm. A 3° wedge is simulated with axisymmetric boundary conditions, yielding a 2D axisymmetric case in OpenFOAM. The volume flow rate is set at the inlet and a constant pressure is set at the outlet. The results using the Launder-Sharma $k - \varepsilon$ and $\overline{v^2} - f$ turbulence models are very similar, as seen in figure 5(a).
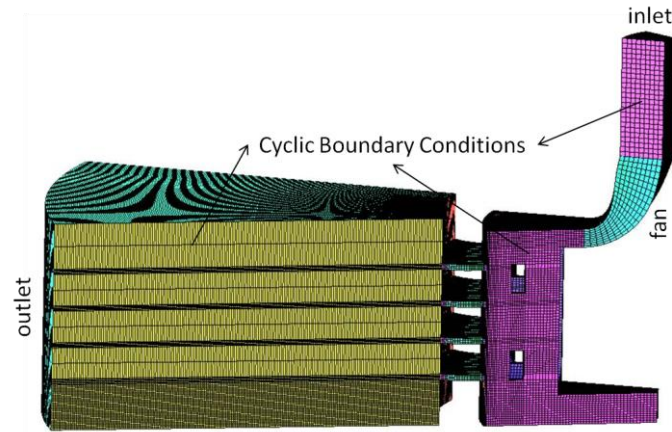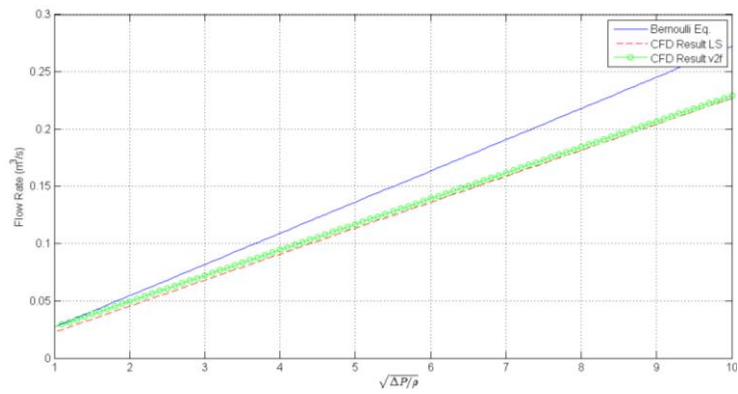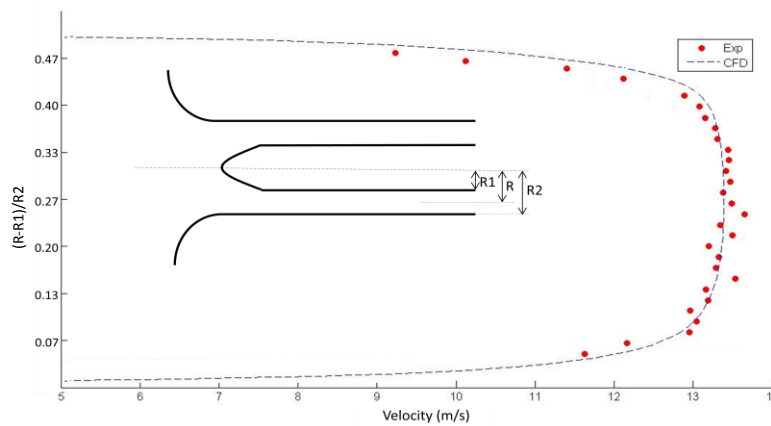
Figure 4 Computational domain, which includes a 1/12th sector of the total geometry

(a)

(b)

Figure 5 (a) Flow rate as a function of square root of pressure difference. The Bernoulli equation curve is plotted as a reference. (b) CFD vs. experimental velocity at the inlet of the fan.

2.2. Fan Design

Previous studies by Moradnia et al. [8-11] showed that the original fan did not give enough pressure build-up and accompanying flow rate, and that there were massive recirculation regions after the fan blades. A new fan is designed in the present work, to resolve these disadvantages and to have better aerodynamic characteristics, see figure 6. New flow passages are also designed. CFD simulations are used in the design process, using the steady-state single rotating reference frame (SRF) modeling in

OpenFOAM. A 1/12 sector of the fan is simulated and the blades are assumed infinitely thin. The final design is manufactured using PolyJet 3D printing, as precision and surface smoothness is important in the fan.

Figure 6 Old fan (left) vs. new fan (right)

2.3. Different Stators

The present study considers three different stator spacer configurations, see figure 7. One has curved spacers, the second one has straight spacers, and the third one has straight spacers with pick-up. All main dimensions of these three stators are the same. The effects of these different stator spacer configurations on the flow distribution are studied numerically. However, the measurements of the present study are restricted to the curved configuration.
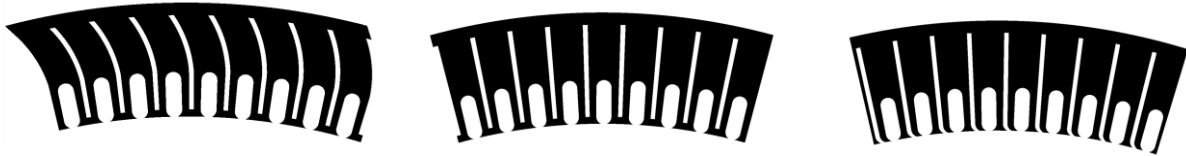

Figure 7 Different stator channels. Left: Curved spacers. Middle: Straight spacers. Right: Straight spacers and pick-up

3. Numerical Modelling

The numerical simulations of the generator model are performed using the OpenFOAM CFD tool, using the steady-state multiple reference frame (MRF) concept. The MRF approach requires that stationary and rotating regions are defined, separated from each other by an axisymmetric interface. The MRF approach does not rotate any part of the mesh. Source terms for the rotation are instead added in the virtually rotating region. This approach has proven to give an appropriate pressure build-up in the stator [8-11]. There is a small effect due to the frozen position of the rotor relative to the stator. However, the results of the MRF approach are considered to meet engineering accuracy.

A low-Re turbulence model is required for modeling the effect of turbulence, due to the small velocities and dimensions in the stator channels. The $\overline{v^2} - f$ turbulence model is used in the present study. The mesh is generated using the ANSYS ICEM CFD mesh generator, keeping the wall y^+ values at about 1. The governing equations are discretized using structured meshes, covering a 1/12 sector in the tangential direction, employing cyclic boundary conditions. The computational domains hence include one rotor pole, one fan blade and nine cooling channels in each channel row. The results are considered converged when the residuals are small and stabilized, the rotor axial torque is stabilized, and the flow rate through the computational domain is stabilized. The numerical results are additionally averaged over a large number of iterations after reaching convergence.

4. Experimental Setup

The experimental part of this work includes 5-hole probe velocity measurement at the inlet of the fan, PIV (LaVision) velocity measurements inside the stator channels, and total pressure measurements at the outlet of the stator channels. Each method is described briefly in the coming paragraphs.

The flow measurements at the inlet are performed using the five-hole pressure probe shown in figure 8(b). The probe is of L-type with a tip diameter of 1.6mm. The probe is calibrated for cone angles from 0 to $52°$. The measurement accuracy is better than 1% for the velocity magnitude and $0.5°$

for the flow angles. A two-axial traversing system is used to spatially position the probe at the generator inlet. The time-mean statistics are evaluated from 2000 samples.

A horizontal PIV measurement plane is used in the stator channels, and the camera is set on the top of the generator. The camera is of the type Imager ProX 4M. It is used with a synchronizing device, and a double-pulsed laser. The camera and laser head are mounted on a single frame, enabling simultaneous traversing of the system without re-adjustment. The system calibration is performed using a standard calibration plate, Type11, provided by LaVision. A smoke generator is utilized to seed the flow with particles of average size 1 μm. The PIV images are processed in the DaVis software. To avoid rig displacements in the PIV measurements, the image capturing is synchronized to the rotor position. Averaging is done over 100 data samples to examine the velocity distribution in the stator channel. In the PIV processing, a 64×64 – 32×32 pixel window with 50% overlapping is used in multi-pass mode. The error in the PIV velocity field is estimated to 0.34 m/s due to the 0.2 pix error in the sub-pixel interpolation.

The outlet flow measurements are performed using a total pressure probe rake positioned at the channel outlets, as shown in figure 8 (a). The rake consists of 14 total pressure tubes. The rake tubes are aligned with the radial direction. The outlet total pressure is averaged over 1000 data samples using a scanning frequency of 500Hz. The values are monitored using a 16-channel PSI 9116 digital pressure scanner from Pressure Systems Inc. The measuring range of the scanner transducers is ±2500Pa. To maintain the highest possible accuracy in a low-pressure range, the pressure transducers are regularly controlled for an offset and reset to zero before each set of measurements. The accuracy of the vertical and horizontal positioning of the rake is 0.5mm. The resulting precision of the transducer offset is better than 0.4Pa, which corresponds to 1.16m/s. The statistical uncertainty of the mean total pressure is 0.86Pa, with 99% confidence in regions with the highest pressure fluctuations (12Pa).

<div align="center">(a)</div> <div align="center">(b)</div>

Figure 8 (a) Total pressure rake installed on a two-axis traverse system, (b) 5-hole pressure probe at the inlet

5. Results

In order to compare the numerical and experimental total pressure distributions at the stator channel outlets, a total pressure coefficient is defined for each individual channel, as

$$C_{pTot} = \frac{(p_{tot} - \overline{p_{tot}})}{(p_{tot,max} - \overline{p_{tot}})} \tag{1}$$

Here p_{tot} is a local total pressure value at the outlet of a channel, $\overline{p_{tot}}$ is the mean total pressure at the outlet of the same channel, and $p_{tot,max}$ is the maximum value of the total pressure at the outlet of the same channel. Figure 9 shows the experimental total pressure coefficient, C_{pTot}, of eight successive channels in different rows of the stator with curved spacers. The flow structure is very similar in all the channels of each row and the flow is axisymmetric as expected. Figure 10 shows the

average profiles of the simulated total pressure coefficient of all nine channels on each row, and the average profiles of the experimental total pressure coefficient of that row. The comparison shows a reasonable agreement between the experimental and numerical results.
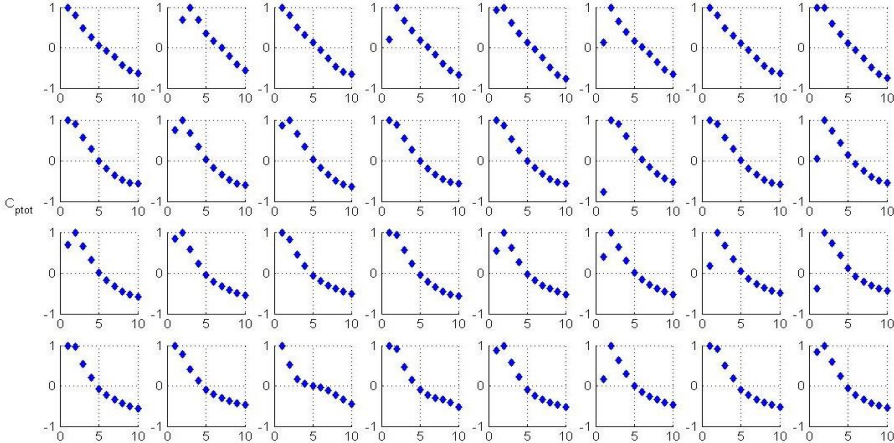

Figure 9 Experimental total pressure coefficient of 8 channels in each row along the channels. Row1: 1st row of stator, Row2: 2nd Row of stator, Row3: 3rd row of stator and Row4:4th row of stator
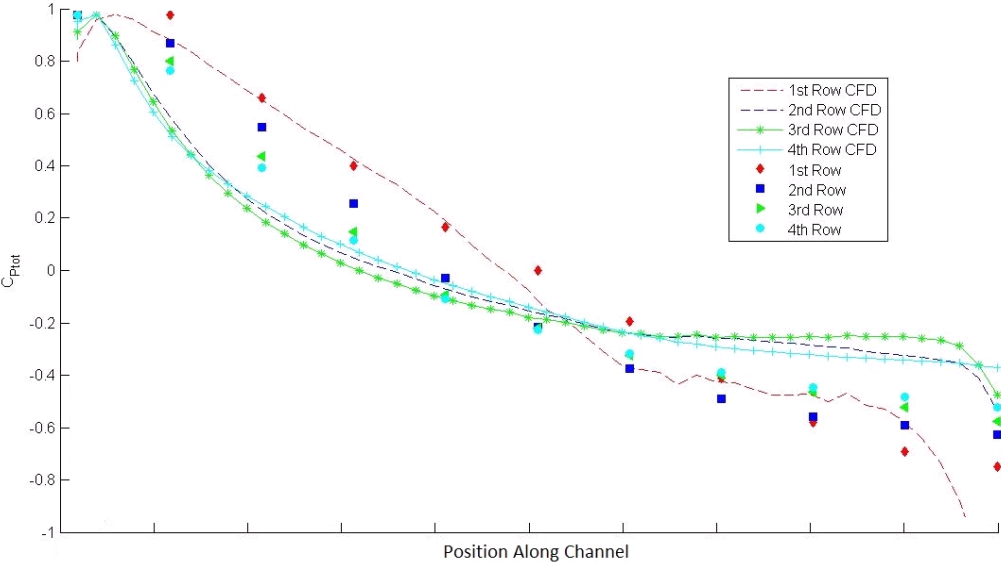

Figure 10 Simulated vs. experimental averaged total pressure coefficient at outlet of stator channel rows

Figure 11 compares the PIV and numerically predicted velocity vectors inside the stator channels. The results are both qualitatively and quantitatively in good agreement. As previously shown by Moradnia [8-11], the flow mainly enters the stator channels on the upstream side of the coils. That is the case also in the present results. However, due to the increased flow rate through the machine, thanks to the new design, the flow on the other side of the coils is here also radially outwards. A detailed analysis of the flow at each side of the coils reveals a 20% difference. A good design should distribute the cooling air as even as possible between the channels and also inside each channel.

Figure 12 shows areas of numerically predicted reverse radial flow in different stator channel configurations. The reverse flow is thus defined as negative radial flow, which means flow toward the rotor axis. All configurations have a positive radial flow at both sides of the coils and reversed flow in the wakes of the coils. The stator with straight spacers have a few additional regions with reversed flow, but the flux difference of the two sides of the coil in less than that for the stator with the curved

spacers. As expected, adding pick-up to the straight spacers makes the flow distribution more even. There is still a small reverse flow zone at the back of the coils, but overall the flow field has the lowest pressure loss and the flattest distribution among the different stator configurations.
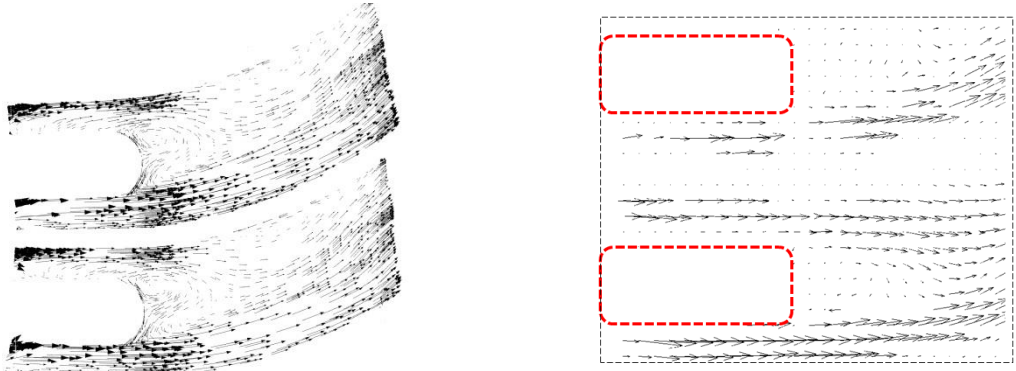

Figure 11 Velocity vectors inside stator channels. Left: Numerical. Right: PIV.
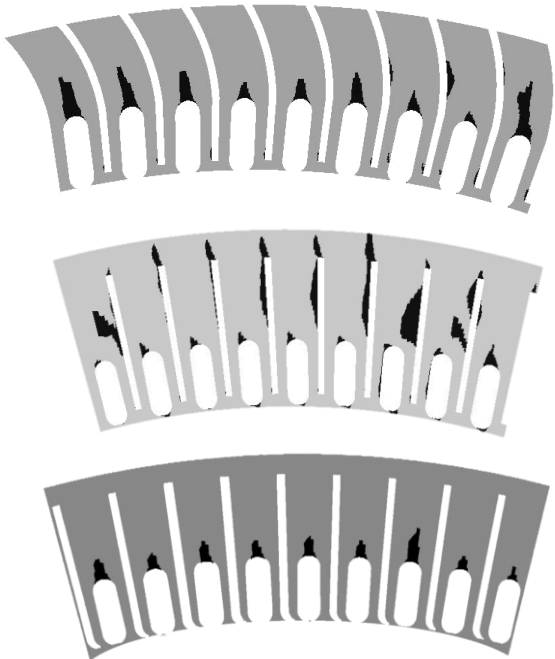

Figure 12 Areas of reverse radial flow. Top: stator with curve spacers. Middle: stator with straight spacers. Bottom: stator with straight spacers and pick-up. The rotation of rotor is counter clockwise in all these cases.

6. Conclusions

The flow of cooling air in a lab model of an electric generator is experimentally studied using PIV measurements inside the stator channels, 5-hole probe measurements at the inlet, and total pressure rake measurements at the outlet of the stator channels. The experimental data is used to validate new numerical simulations of the flow field. The simulations are performed using the steady-state multiple references frame approach, also referred to as *frozen rotor*. The investigations are done under cold conditions, since the present focus is on the flow characteristics of the cooling air inside an electric generator.

The numerically predicted flow features agree very well with the experimental results at all experimental sections, and the numerical approach may be considered useful for developing a better

understanding of the flow of cooling air in electric generators. The flow field inside the stator channels with pick-up is more even, and the losses are lower, than for the stators without pick-up. The study shows that the flow properties can be improved with small changes like the addition of pick-up.

7. Acknowledgments

References
[1] Traxler-Samek G, Zickermann R and Schwery A 2008 Advanced calculation of temperature rises in large air-cooled hydro-generators *Electrical Machines 2008 ICEM 2008 18th Int. Conf. on vol.* 1 pp 1-6.
[2] Boglietti A, Cavagnino A, Staton D, Shanel M, Mueller M and Mejuto C 2009 Evolution and modern approaches for thermal analysis of electrical machines *Industrial Electronics IEEE Transactions* **56** 871-882.
[3] Pasha A A, Hussain M and Gunubushanam N 2010 Experimental and CFD analysis of hydrogenerator stator *Proc. of the 37th National & 4th Int. Conf. on Fluid Mechanics and Fluid Power (Madras, Chennai, India, 16-18 December)*
[4] Zhang Q F, Yan J L, Wang M and Chen Z X 2012 CFD Application on Ventilation System of Hydro-generator. *Advanced Materials Research* **383** 3561-65.
[5] Toussaint K, Torriano F, Morissette J F, Hudon C and Reggio M 2011 CFD analysis of ventilation flow for a scale model hydrogenerator *ASME 2011 Power Conf. collocated with JSME ICOPE 2011* pp 627-637.
[6] Pickering S J, Lampard D and Shanel M 2001 Modelling ventilation and cooling of the rotors of salient pole machines *Electric Machines and Drives Conference 2001 IEMDC 2001 IEEE Int.* pp 806-808.
[7] Gunabushanam N and Suresh J 2006 Experimental and CFD analysis of hydrogenerator ventilation components *Proc.s CIGRE Session*.
[8] Moradnia P, Golubev M, Chernoray V and Nilsson H 2014 Flow of cooling air in an electric generator model–An experimental and numerical study *J. Applied Energy* **114** 644-653.
[9] Moradnia P and Nilsson H 2011 A parametric study of the air flow in an electric generator through stepwise geometry modifications *ECCOMAS Thematic Conf. CFD and Optimization*.
[10] Moradnia P, Chernoray V and Nilsson H 2011 Experimental and numerical investigation of the cooling air flow in an electric generator *HEFAT 2011 8th Int. Conf. on Heat Transfer, Fluid Mechanics and Thermodynamics* pp 242-249.
[11] Moradnia P, Chernoray V and Nilsson H 2014 Experimental assessment of a fully predictive CFD approach, for flow of cooling air in an electric generator *J. Applied Energy* **124** 223-230.